Terahertz Sum-Frequency Excitation of Coherent Optical Phonons in the Two-Dimensional Semiconductor WSe_2

Satoshi Kusaba,[1, 2, a)] Haw-Wei Lin,[3, a)] Ryo Tamaki,[1] Ikufumi Katayama,[1, 4] Jun Takeda,[1, 4, b)] and Geoffrey A. Blake[2, 3, b)]

[1)]*Department of Physics, Graduate School of Engineering Science, Yokohama National University, Yokohama, 240-8501 Japan*

[2)]*Division of Geological and Planetary Sciences, California Institute of Technology, Pasadena, California 91125, USA*

[3)]*Division of Chemistry and Chemical Engineering, California Institute of Technology, Pasadena, California 91125, USA*

[4)]*Semiconductor and Quantum Integrated Electronics Research Center, Institute for Multidisciplinary Sciences, Yokohama National University, Yokohama, 240-8501 Japan*

(*Electronic mail: gab@caltech.edu)

(*Electronic mail: jun@ynu.ac.jp)

(Dated: 22 February 2024)

Driving fundamental excitations via strong light fields is one of the most important issues in solid state physics, which opens up new avenues to control material properties. Two-dimensional materials are fruitful platforms for future semiconductor applications including opto-electric and phononic devices, yet the phonon dynamics and nonlinear phonon-phonon coupling remain under-explored. Here, we demonstrate coherent phonon excitation in thin films of the layered two-dimensional semiconductor WSe_2 induced by intense and broadband ultrafast THz pulses. We performed terahertz Kerr effect spectroscopy and observed coherent phonon oscillations assigned to the E_{2g} optical phonon mode. The phonon amplitude displays a quadratic THz field strength dependence, indicating a sum-frequency THz excitation process. Further, pump-probe polarization and crystal orientation relationships, supported by symmetry analysis of the nonlinear susceptibility and Raman tensors, provide helpful insights into nonlinear phonon-phonon interactions and potential coherent control schemes for the manipulation of phonon polarization and material properties in WSe_2.

Layered semiconductor transition metal dichalcogenides, TMDs, are promising platforms for condensed matter physics because of their unique properties. They are semiconductors with layer-dependent band structures[1,2], in contrast to (semi)metalic graphene or graphite.The monolayers, which consist of one transition metal atom layer and two chalcogen atom layers, have thicknesses of less than 1 nm and are close-to-ideal 2D direct-gap semiconductor crystals. The monolayers have broken inversion symmetry which leads to non-trivial spin-valley coupling[3], valley-dependent circular polarization selection rules[4–6], and chiral phonons carrying angular momentum[7,8]. Their ultimate thinness also lead to strongly-bound and stable excitonic states with binding energies of a few hundred meV[9–11]. Their multilayer or bulk counterparts, which are easily manufactured through mechanical exfoliation, have also attracted significant attention as they retain many of the favorable semiconductor properties of monolayer TMDs, including room temperature valley polarization[12–14]. In addition, heterostructures can be easily fabricated by overlapping two different mono- or multilayer TMDs[15], which enables new opto-electronic devices, so called "twistronics"[16–18], where it is possible to control the electronic and phonic properties, such as Moiré excitons[19] and phonons[20].

Recently, the advancement of intense ultrafast infrared light sources has enabled research into strongly-driven carrier dynamics and elementary excitations such as excitons and phonons[21–29]. Thin TMD crystals are one of the most popular platforms due to the aforemetioned properties and negligible propagation effects. Under the irradiation of strong mid-infrared (MIR) pulses (from $\sim$ 10 to $\sim$ 100 THz), high harmonics generation from coherently driven valley carriers have been observed, demonstrating promise as a new light source and a platform for attosecond physics[23,25–27], while recent experiments have further highlighted the possibility to control excitonic quantum states in TMDs with intense MIR radiation[29]. On the other hand, in the lower frequency region (from $\sim$ 1 to $\sim$ 10 THz), i.e., the far-infrared (FIR) or THz region, previous Raman and coherent phonon spectroscopies in the visible and near-IR (NIR) wavelengths[30,31] have revealed numerous optical phonon modes near $\sim$ 10 THz in TMDs. These techniques employ light sources that are non-resonant with the phonon degrees of freedom, which have a limited ability to drive coherent dynamics and nonlinear interactions involving phonon modes. In contrast, efficient excitation of both IR- and Raman-active phonon modes can be achieved with a broadband THz pulse through a number of electric dipole- and polarizability-mediated excitation mechanisms[32]to enable a comprehensive investigation of the THz phonon dynamics in TMDs, including excitation mechanism[33,34], phonon-phonon couplings[21], and anharmonicities[35]. To date, THz spectroscopic studies on TMDs have mainly focused on the carrier dynamics at lower frequency around 1 THz[36–38], and broadband THz light

[a)] Authors contributed equally.
[b)] Authors to whom correspondence should be addressed: gab@caltech.edu and jun@ynu.ac.jp .

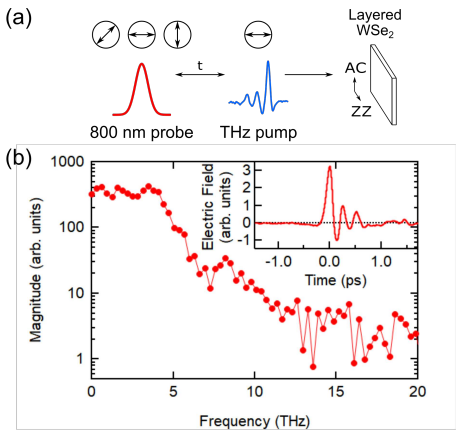

FIG. 1. (a) Pulse sequence of the TKE experiment. The polarization of the THz pump and 800 nm probe pulses are shown in the circles. (b) Bandwidth and pulse shape (inset) of the THz pump pulse.

sources have not been employed to investigate driven phonon dynamics under strong THz excitation.

Here, we report direct observation of coherent optical phonon oscillations in free-standing thin bulk TMDs under intense and broadband ultrafast THz pulsed irradiation. The phonon structure of the bulk TMDs very closely resembles that of their monolayer counterparts[14]. The free-standing bulk samples also eliminate interfering substrate effects. We specifically performed THz Kerr effect (TKE) spectroscopy, or THz-pump-optical-Kerr-rotation-probe spectroscopy[39–41], in bulk WSe_2 thin films, one of the TMDs. In addition to signals attributed to relaxation of thermalized electron population, we observed oscillatory signals with frequencies of $7 \sim 8$ THz, which we attribute to the E_{2g} optical phonon modes. The oscillation amplitude is proportional to the square of the THz electric field strength, which suggests that the coherent optical phonons are excited by a sum-frequency (SF) THz excitation process. Next, we performed symmetry analysis of the nonlinear susceptibility tensor $\chi^{(3)}$ and the Raman tensor R, which are both consistent with results from the polarization dependence measurements. Finally, we present a quantum mode-specific picture of the SF THz excitation process via the polarizability operator. Alternative excitation mechanisms, including nonlinear phonon-phonon coupling[32,33] and carrier-phonon coupling[30,31], are discussed and ruled out.

A schematic of the TKE experiment is shown in Fig. 1(a) (see the SI for a full description of the experimental setup). The few-cycle broadband ultrafast THz pulse is generated by pumping a 4–N,N–dimethylamino–4'–N'–methyl–stilbazolium 2,4,6–trimethylbenzenesulfonate (DSTMS) crystal (Swiss Terahertz) with the 250 μJ, 1.4 μm output from a TOPAS-C optical parametric amplifier (Light Conversion). The THz pulse shape and bandwidth are characterized with electro-optic sampling (EOS) on 100 μm GaP[42] and shown in Fig. 1(b), where the THz pulse duration is ~600 fs and the bandwidth extends up to ~10 THz (-20 dB). The peak THz field strength is estimated from EOS to be $>$ 500 kV/cm. The THz-induced optical anisotropy is probed by a weak 40 fs 800 nm pulse, which experiences a small angle rotation of the polarization. The rotated polarization component is isolated by a crossed analyzing polarizer and detected with a photodiode. The polarization of the THz pulse is parallel to either the armchair (AC) or zigzag (ZZ) direction of the WSe_2 sample (see Fig. 2(a) for description of the possible lattice orientations). The polarization of the probe pulse is set to 0°, 45°, or 90° relative to that of the THz pulse.

Thin free-standing WSe_2 single-crystals were obtained by mechanical exfoliation using adhesive tape with a $\sim$ 1 mm square hole. The crystal/tape assembly are fixed on a 400 μm diameter pinhole (Fig. 2(b)) to detect only the THz-irradiated area. The typical single-crystal size is $1 \sim 2$ mm, which fully covers the pinhole. The sample thicknesses were estimated to be a few hundred nm from the interference fringes in the optical transmittance spectrum (see the SI for details). The thickness of the WSe_2 samples are carefully chosen such that they are sufficiently thin to be transparent at the 800 nm probe wavelength, while sufficiently thick to accumulate enough phase difference from the THz-induced weak transient birefringence.

The crystal structure of WSe_2 is shown in Fig. 2(a), where two specific in-plane axes, known as the AC and ZZ directions, are shown by the red and blue arrows. The crystal orientation was determined by polarization-resolved second harmonic generation (SHG) spectroscopy[43]. Because WSe_2 only possesses mirror symmetry along the ZZ direction but not the AC direction, the polarization-dependent SHG amplitude was used to assign the AC and ZZ directions of the crystal (see the SI for details).

The unit cell of bulk TMDs contains 6 atoms. Normal mode analysis indicates that there are 3 acoustic and $6 \times 3 - 3 = 15$ optical phonon modes, respectively. Accounting for mode degeneracy, the optical phonon modes are classified into 2 IR-active modes ($1A_{2u} + 2E_{1u}$), 4 Raman-active modes ($1A_{1g} + 2E_{1g} + 4E_{2g}$) and 4 inactive modes ($B_{1u} + 2B_{2g} + 2E_{2u}$). The lattice motions of the IR- and Raman-active optical phonon modes in WSe_2 are shown in Fig. 2(c). We performed Raman spectroscopy (Fig. 2(d)) to measure and assign the phonon modes frequencies of WSe_2 in the THz range. Linearly polarized light (532 nm), parallel to either the ZZ or AC direction, was incident on the WSe_2 sample, and both the polarized and depolarized Raman scattering photons are detected. The features were identical for the two crystal orientations (see Fig S3 in the SI).We observe two main peaks at $\sim$ 250 cm^{-1} ($\sim$ 7.5 THz). The lower energy peak at 248 cm^{-1} is attributed to the A_{1g} and/or E^1_{2g} modes, whose phonon frequencies are nearly identical[44,45]. The higher energy peak at 258 cm^{-1} is attributed to the second order Raman response of acoustic phonons at the Brillouin zone edge (the $2LA$(K)[31] or $2LA$(M)[44,45] modes). Additional small peaks at 138 cm^{-1}, 359 cm^{-1}, 372 cm^{-1}, and 393 cm^{-1} are also second-order Raman peaks[44,45]. Critically, our broadband THz pulse may, in

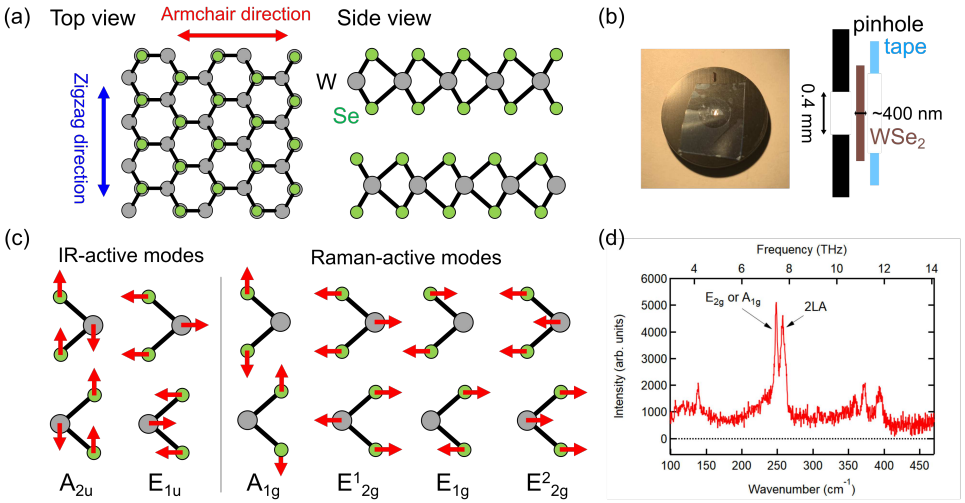

FIG. 2. (a) Crystal structure of layered WSe_2 viewed from the top and side. (b) Image and schematic of the WSe_2 sample mounted on a 400 μm pinhole. (c) The symmetry and lattice motions of Raman- and IR-active phonon modes. (d) Micro-Raman spectra $(X(Z\bar{Z})X+X(Z\bar{Z})Y)$ of the WSe_2 sample.

theory, excite Raman-active modes of up to 20 THz via a number of SF and difference-frequency (DF) THz photonic and phononic excitation processes[32], suggesting potential THz-driven dynamics upon intense THz excitation. We note that in the TKE experiment, the THz pump pulse propagates normal to the sample plane, leading to phonon excitations at only the Γ point. This suppresses second-order Raman features at Brillouin zone edges. Further, the crossed-polarized detection scheme employed in TKE spectroscopy detects only the depolarized Raman scattered photons. Thus, TKE spectroscopy cannot detect totally symmetric modes (A_{1g}) and is only sensitive to anisotropic modes, such as the E_{2g} mode.

To explore driven-phonon dynamics in TMDs, the WSe_2 sample was subject to intense broadband ultrafast THz pulses that span 1-10 THz. The induced dynamics were probed using a Kerr effect heterodyne detection setup, which is directly sensitive to the transient anisotropy induced by coherently excited phonon oscillations [46,47]. Figure 3 shows the TKE signal of WSe_2, where the polarization of both the THz and probe pulses are parallel to the AC direction. The measured TKE signal consists of two main features: an oscillatory signal and an exponential decay component. The exponential decay component was fitted by a bi-exponential function, yielding $\sim$ 100 fs (fast) and $\sim$ 400 fs (slow) decay components. Within the THz pulse duration, similar features in TKE spectroscopy with below-bandgap probing are generally assigned to an instantaneous nonlinear polarization from the third-order nonresonant electronic polarizability[48]. However, the observed signal shows a longer relaxation time than that expected from the THz pulse shape (Fig. 1(b)) and the thinness of the single-crystal samples in this work ($\sim$500 nm). Concrete assignment of this feature is beyond the focus of this work and requires further investigations.

Subtraction of the exponential component isolates the oscillatory signal, as shown by the green difference trace in Fig. 3. The Fourier transform (FT) spectra of the oscillatory signal is shown in the inset of Fig. 3 and reveals a clear $\sim$ 7.5 THz peak, which matches the frequency of the E_{2g} and A_{1g} phonon modes. As described previously, TKE spectroscopy is only sensitive to anisotropic vibrational modes. Thus, we attribute the observed oscillatory signal to transient anisotropy induced by coherently excited vibrational oscillations of the E_{2g} symmetry phonon mode.

To further elucidate the excitation mechanism of the observed E_{2g} phonon oscillations, TKE signals at different THz pump field strengths were measured, as shown in Fig. 4(a). The corresponding FT spectra are shown in Fig. 4(b). Two regions of interest in the frequency spectra are analyzed, namely, the electronic response (1-2 THz) and the coherent excitation of the E_{2g} phonon oscillations (7-8 THz). The region between 0 to 1 THz was avoided due to higher potential of systematic noise contributions. The integrated FT amplitudes in these two regions as a function of THz field strength are shown in Fig. 4(c) and 4(d), where both features show clear quadratic dependence relative to the input THz pump electric field. At below $\sim$30% of maximum THz field strength, detection of the coherent phonon signal above noise becomes challenging, leading to the plateau in amplitude in Fig. 4(d). The quadratic field strength dependence of the E_{2g} phonon mode directly indicates that the excitation in-

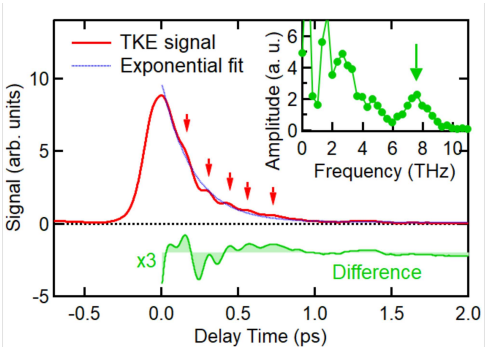

FIG. 3. TKE signal from layered WSe_2 (red) where the polarization of the THz and probe pulses are parallel to the AC direction. The exponential decay component is subtracted (see main text for details) to reveal the coherent oscillations (green). The corresponding FT of the difference signal is shown in the inset, where the ~ 7.5 THz E_{2g} phonon mode is labelled.

volves two THz photon interactions, which we attribute to a SF excitation process with two THz photons. Such photonic SF THz excitation processes have also been observed in both solids (diamond)[24] and liquids (halogenated methane)[34].

Below, we consider all possible THz excitation mechanisms of a Raman-active phonon mode to justify our assignment of the photonic SF THz mechanism. As described in detail by Maehrlein and coworkers[32], a Raman-active phonon mode may be excited by SF and DF processes that are either photonic or ionic in nature. Importantly, all four processes leads to an empirical quadratic THz field strength dependence. Ionic scattering concerns the excitation of Raman-active phonon modes through nonlinear coupling of two IR-active phonon modes, whose SF or DF component matches that of the Raman-active mode. This process is sometimes also referred to as the quadratic-linear or trilinear coupling of phonon modes[33,46]. The nonlinear coupling interaction is generally described with the term $\propto q_{IR}^2 q_R$, where q_{IR} and q_R are the coordinate of the IR- and Raman-active oscillators respectively. Such processes require both symmetry and energy matching to occur. The IR-active phonon modes in WSe_2 are of A_{2u} and E_{1u} symmetry, therefore, the relevant symmetry products are $\langle E_{2g}|A_{2u}E_{1u}\rangle$, $\langle E_{2g}|E_{1u}E_{1u}\rangle$, and $\langle E_{2g}|A_{2u}A_{2u}\rangle$. Only $\langle E_{2g}|E_{1u}E_{1u}\rangle \supset A_{1g}$ is symmetry allowed. However, the E_{1u} phonon modes in WSe_2 have almost identical energies as do the E_{2g} phonon modes. As a result, the SF and DF nonlinear coupling of two E_{1u} phonons to one E_{2g} phonon cannot occur due to conservation of energy, ruling out both the SF and DF ionic scattering mechanisms. We also note that excitation of the E_{2g} mode through electron-phonon coupling mechanisms are unlikely because the THz photon energy (< 40 meV) is substantially lower than the bandgap of WSe_2 (1.2 eV)[49,50].

On the other hand, photonic Raman scattering describes coherent excitation of phonons driven by the square of the electric field of the incident photons. This includes the familiar impulsive stimulated Raman scattering (ISRS), which uses the DF component, and the SF THz excitation mechanism assigned here. Given the THz pulse bandwidth in this work, we can quantify the available SF and DF THz power that could drive the excitation of the E_{2g} phonon modes at 7.5 THz for WSe_2 (see Fig. S5 in the SI for details), which reveal that the THz SF component is more than 11-fold higher than the THz DF component, strongly suggesting SF THz excitation to be the primary mechanism for the coherent phonon oscillation observed. The distinction between ISRS and THz SF excitation mechanisms is crucial for coherent control of phonon modes because THz SF excitation is sensitive to the carrier envelope phase (CEP) of the incident THz pulse, which enables additional control of the phase of the lattice vibration[24].

Next, we investigate the field polarization dependence of the excited coherent oscillations and electronic signal. Fig. 5(a) shows the pump-probe polarization angle dependence of the TKE signal where the THz pump polarization is parallel to the AC crystal direction and the relative angle between the THz pump and 800 nm probe polarization are 0°, 45°, and 90°. These experiments are conducted by only rotating the probe polarization with all other conditions fixed. A clear enhancement of signal is observed when the probe polarization is set at 45° relative to that of the THz pump. The TKE signal is identical when the pump-probe angle is 0° or 90°. In contrast to the signal in Fig. 3, those in Fig. 5 were obtained with fully-crossed polarizers in the detection setup, which minimized the local oscillator to eliminate nonlinear amplitude scaling of the heterodyne detection scheme and reduce noise from laser intensity fluctuations. As shown in Fig. 4(c), the electronic relaxation feature is proportional to the square of the THz electric field, indicating that the signal is third-order in nature. The nonlinear polarization $P_i^{(3)}$ induced and detected in the TKE setup is given as

$$P_i^{(3)} = \chi_{ijkl}^{(3)} E_j E_k E_l \tag{1}$$

where E_j is the probe polarization and E_k and E_l the THz pump polarization. Considering the symmetry group of layered WSe_2 (D_{6h}), selection rules predict that the nonlinear polarization vanishes at 0° or 90° and is maximized at 45° pump-probe polarization angles (see the SI for details). The non-zero TKE signal observed at 0° or 90° are likely due to slight ellipticity of the THz polarization state near the focus that are inherent to off-axis parabolic mirrors[51], which are employed in this work to achieve the intense THz field strengths. On the other hand, Fig. 5(b) shows the TKE signals of WSe_2 with the THz polarization parallel to the AC and ZZ crystal axis, respectively. The probe polarization is kept at $+45°$ relative to the THz polarization, and the experimental conditions are achieved by rotating the sample. Clearly, the excited coherent phonon oscillations are the same frequency of ~ 7.5 THz with identical phase, suggesting the same E_{2g} mode is excited. Given the SF excitation mechanism, which proceeds through the polarizability operator, polarization dependence of the coherent phonon oscillations are analyzed by considering Raman selection rules. The Raman scattering intensity I

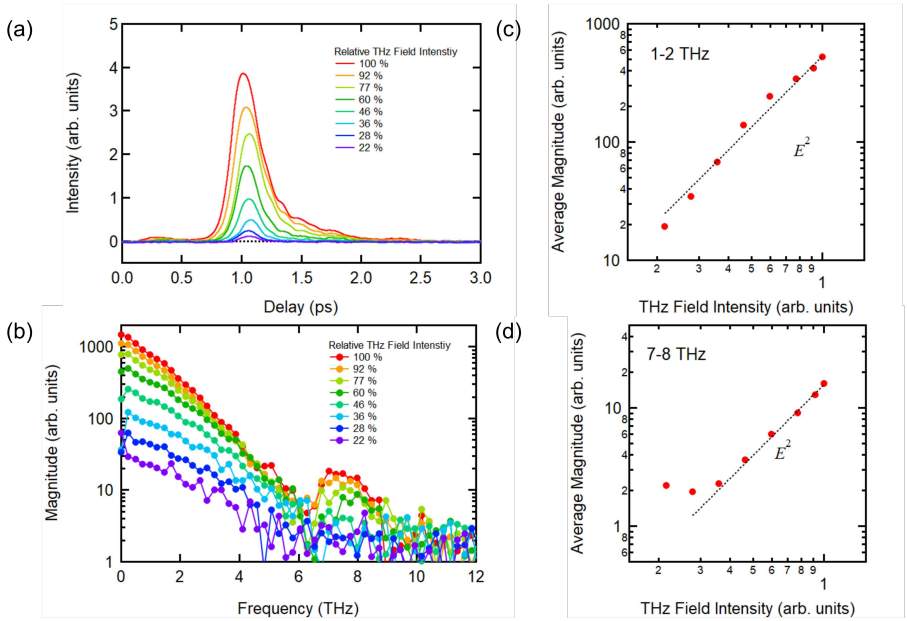

FIG. 4. (a) The WSe_2 TKE signal measured at different THz pump field strengths and (b) the corresponding FT spectra. THz field strength dependence of the FT magnitudes between (c) 1-2 THz and (d) 7-8 THz.

of a vibrational mode is given as

$$I \propto |e_i \cdot R \cdot e_d|^2 \tag{2}$$

where e_i and e_d are the incident and detected photons respectively and R is the Raman scattering tensor of the mode. Accounting for the symmetry of the WSe_2 lattice (see the SI for details), the polarization selection rule for SF THz excitation of the E_{2g} mode is $\Phi = 2\phi$, where ϕ and Φ are the polarization angle of the THz pulse and phonon oscillation, respectively (where the AC direction is defined as 0°). Specifically, excitation with both THz polarization parallel to the AC (0°) and ZZ (90°) direction induces E_{2g} phonons along the AC direction, which is consistent with our experimental result. We note that the derived polarization relations also suggest that the phonon signal is maximized when the pump-probe angle is 45°, which agrees with the data in Fig. 5(a). The derived polarization selection rule is analogous to SHG processes and distinct from dipole-allowed one-photon processes, which highlights the importance of determining excitation mechanisms for driven phonon dynamics in coherent control schemes.

In summary, we demonstrate strongly-driven coherent phonon dynamics in layered semiconductor WSe_2 induced by intense broadband ultrafast THz irradiation. In addition to the thermalized electron response, we directly observe oscillatory signals with a lifetime of ~ 1 ps, which we attribute to

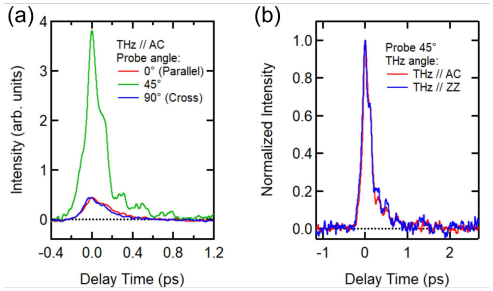

FIG. 5. TKE signal of layered WSe_2 measured with different (a) probe and (b) pump polarization conditions.

coherently-excited oscillations of the E_{2g} phonon mode. The oscillation amplitude displays quadratic THz field strength dependence, which indicates that the excitation mechanism is a sum-frequency (two-photon) process. We discuss and rule-out alternative mechanisms of excitation, including nonlinear phonon-phonon coupling and electron-phonon coupling. Our symmetry analysis of the nonlinear susceptibility tensor $\chi^{(3)}$ and Raman tensor R, together with experimental polarization dependence results, reveal detailed relationships and selection

rules between excitation/detection polarization, crystal orientation, and phonon oscillation direction. Our results provide helpful mechanistic insights into the driven-dynamics and coherent control of phonons by strong THz fields in solid materials. This work also serves as the foundation for further investigations into nonlinear phonon-phonon coupling dynamics through multidimensional THz techniques, such as 2D THz spectroscopy[52] and hybrid THz spectroscopy[35].

SUPPLEMENTARY MATERIAL

See the supplementary material for descriptions of the experimental setup of the TKE spectrometer, preparation and characterization of the WSe_2 samples with SHG and micro-Raman spectroscopies, and complete symmetry analysis of the nonlinear susceptibility and Raman tensors of WSe_2.

AUTHOR'S CONTRIBUTIONS

S.K. and H.W.L. conceived the project, J.T. and G.A.B. supervised the project. S.K. prepared the WSe_2 samples. H.W.L. prepared the TKE spectrometer. S.K. and H.W.L. performed the experiments, data analysis, and symmetry analysis. All authors discussed and prepared the manuscript.

ACKNOWLEDGMENTS

H.W.L. acknowledges financial support from the Ministry of Education of Taiwan. H.W.L and G.A.B acknowledge support by the National Science Foundation CSDM-A program (Grant No. CHE-1665467) and NASA APRA program (Grant No. 80NSSC21K1467). S.K and J.T. acknowledge support by the Grants for Bilateral Collaborations (No. 120209911) and the Grants-in-Aid for Scientific Research (Nos. 20H05662, 22K20354, 23K13043).

CONFLICT OF INTEREST

The authors declare no conflicts of interest.

DATA AVAILABILITY STATEMENT

The data that support the findings of this study are available from the corresponding author upon reasonable request.

REFERENCE

[1] A. Splendiani, L. Sun, Y. Zhang, T. Li, J. Kim, C.-Y. Chim, G. Galli, and F. Wang, Nano Letters **10**, 1271 (2010).
[2] K. F. Mak, C. Lee, J. Hone, J. Shan, and T. F. Heinz, Physical Review Letters **105**, 136805 (2010).
[3] D. Xiao, G.-B. Liu, W. Feng, X. Xu, and W. Yao, Physical Review Letters **108**, 196802 (2012).
[4] K. F. Mak, K. He, J. Shan, and T. F. Heinz, Nature Nanotechnology **7**, 494 (2012).
[5] H. Zeng, J. Dai, W. Yao, D. Xiao, and X. Cui, Nature Nanotechnology **7**, 490 (2012).
[6] T. Cao, G. Wang, W. Han, H. Ye, C. Zhu, J. Shi, Q. Niu, P. Tan, E. Wang, B. Liu, and J. Feng, Nature Communications **3**, 887 (2012).
[7] L. Zhang and Q. Niu, Physical Review Letters **115**, 115502 (2015), arXiv:1502.02573v1.
[8] H. Zhu, J. Yi, M.-Y. Li, J. Xiao, L. Zhang, C.-W. Yang, R. A. Kaindl, L.-J. Li, Y. Wang, and X. Zhang, Science **359**, 579 (2018).
[9] A. Chernikov, T. C. Berkelbach, H. M. Hill, A. Rigosi, Y. Li, O. B. Aslan, D. R. Reichman, M. S. Hybertsen, and T. F. Heinz, Physical Review Letters **113**, 076802 (2014).
[10] A. V. Stier, N. P. Wilson, K. A. Velizhanin, J. Kono, X. Xu, and S. A. Crooker, Physical Review Letters **120**, 057405 (2018).
[11] S. Kusaba, Y. Katagiri, K. Watanabe, T. Taniguchi, K. Yanagi, N. Naka, and K. Tanaka, Optics Express **29**, 24629 (2021).
[12] R. Suzuki, M. Sakano, Y. J. Zhang, R. Akashi, D. Morikawa, A. Harasawa, K. Yaji, K. Kuroda, K. Miyamoto, T. Okuda, K. Ishizaka, R. Arita, and Y. Iwasa, Nature Nanotechnology **9**, 611 (2014).
[13] B. Zhu, H. Zeng, J. Dai, Z. Gong, and X. Cui, Proceedings of the National Academy of Sciences **111**, 11606 (2014).
[14] Q. Cai, B. Wei, Q. Sun, A. H. Said, and C. Li, Materials Today Physics **28**, 100856 (2022).
[15] A. K. Geim and I. V. Grigorieva, Nature **499**, 419 (2013).
[16] B. Hunt, J. D. Sanchez-Yamagishi, A. F. Young, M. Yankowitz, B. J. LeRoy, K. Watanabe, T. Taniguchi, P. Moon, M. Koshino, P. Jarillo-Herrero, and R. C. Ashoori, Science **340**, 1427 (2013).
[17] Y. Cao, V. Fatemi, S. Fang, K. Watanabe, T. Taniguchi, E. Kaxiras, and P. Jarillo-Herrero, Nature **556**, 43 (2018).
[18] Y. Cao, V. Fatemi, A. Demir, S. Fang, S. L. Tomarken, J. Y. Luo, J. D. Sanchez-Yamagishi, K. Watanabe, T. Taniguchi, E. Kaxiras, R. C. Ashoori, and P. Jarillo-Herrero, Nature **556**, 80 (2018).
[19] H. Yu, G.-B. Liu, J. Tang, X. Xu, and W. Yao, Science Advances **3**, 1 (2017).
[20] M.-L. Lin, Q.-H. Tan, J.-B. Wu, X.-S. Chen, J.-H. Wang, Y.-H. Pan, X. Zhang, X. Cong, J. Zhang, W. Ji, P.-A. Hu, K.-H. Liu, and P.-H. Tan, ACS Nano **12**, 8770 (2018).
[21] M. Rini, R. Tobey, N. Dean, J. Itatani, Y. Tomioka, Y. Tokura, R. W. Schoenlein, and A. Cavalleri, Nature **449**, 72 (2007).
[22] T. Kampfrath, K. Tanaka, and K. A. Nelson, Nature Photonics **7**, 680 (2013).
[23] H. Liu, Y. Li, Y. S. You, S. Ghimire, T. F. Heinz, and D. A. Reis, Nature Physics **13**, 262 (2017).
[24] S. Maehrlein, A. Paarmann, M. Wolf, and T. Kampfrath, Physical Review Letters **119**, 127402 (2017).
[25] N. Yoshikawa, T. Tamaya, and K. Tanaka, Science **356**, 736 (2017).
[26] S. Ghimire and D. A. Reis, Nature Physics **15**, 10 (2019).
[27] N. Yoshikawa, K. Nagai, K. Uchida, Y. Takaguchi, S. Sasaki, Y. Miyata, and K. Tanaka, Nature Communications **10**, 3709 (2019).
[28] K. Uchida, K. Nagai, N. Yoshikawa, and K. Tanaka, Physical Review B **101**, 094301 (2020).
[29] K. Uchida, S. Kusaba, K. Nagai, T. N. Ikeda, and K. Tanaka, Science Advances **8**, 1 (2022).
[30] T. Y. Jeong, B. M. Jin, S. H. Rhim, L. Debbichi, J. Park, Y. D. Jang, H. R. Lee, D.-H. Chae, D. Lee, Y.-H. Kim, S. Jung, and K. J. Yee, ACS Nano **10**, 5560 (2016).
[31] S. Bae, K. Matsumoto, H. Raebiger, K.-i. Shudo, Y.-H. Kim, Ø. S. Handegård, T. Nagao, M. Kitajima, Y. Sakai, X. Zhang, R. Vajtai, P. Ajayan, J. Kono, J. Takeda, and I. Katayama, Nature Communications **13**, 4279 (2022).
[32] D. M. Juraschek and S. F. Maehrlein, Phys. Rev. B **97**, 174302 (2018).
[33] C. L. Johnson, B. E. Knighton, and J. A. Johnson, Physical Review Letters **122**, 73901 (2019).
[34] G. Mead, H.-W. Lin, I.-B. Magdău, T. F. Miller, and G. A. Blake, The Journal of Physical Chemistry B **124**, 8904 (2020).
[35] H.-W. Lin, G. Mead, and G. A. Blake, Physical Review Letters **129**, 207401 (2022).

[36]C. H. Lui, A. J. Frenzel, D. V. Pilon, Y.-H. Lee, X. Ling, G. M. Akselrod, J. Kong, and N. Gedik, Physical Review Letters **113**, 166801 (2014).
[37]C. J. Docherty, P. Parkinson, H. J. Joyce, M.-H. Chiu, C.-H. Chen, M.-Y. Lee, L.-J. Li, L. M. Herz, and M. B. Johnston, ACS Nano **8**, 11147 (2014).
[38]X. Yan, L. Zhu, Y. Zhou, Y. E, L. Wang, and X. Xu, Applied Optics **54**, 6732 (2015).
[39]M. C. Hoffmann, N. C. Brandt, H. Y. Hwang, K. L. Yeh, and K. A. Nelson, Applied Physics Letters **95**, 2007 (2009), arXiv:0907.5081.
[40]A. A. Melnikov, Y. G. Selivanov, and S. V. Chekalin, Physical Review B **102**, 224301 (2020).
[41]G. Mead, I. Katayama, J. Takeda, and G. A. Blake, Review of Scientific Instruments **90**, 053107 (2019).
[42]A. Leitenstorfer, S. Hunsche, J. Shah, M. C. Nuss, and W. H. Knox, Applied Physics Letters **74**, 1516 (1999).
[43]N. Kumar, S. Najmaei, Q. Cui, F. Ceballos, P. M. Ajayan, J. Lou, and H. Zhao, Physical Review B **87**, 161403 (2013).
[44]W. Zhao, Z. Ghorannevis, K. K. Amara, J. R. Pang, M. Toh, X. Zhang, C. Kloc, P. H. Tan, and G. Eda, Nanoscale **5**, 9677 (2013).
[45]E. del Corro, H. Terrones, A. Elias, C. Fantini, S. Feng, M. A. Nguyen, T. E. Mallouk, M. Terrones, and M. A. Pimenta, ACS Nano **8**, 9629 (2014).
[46]A. A. Melnikov, K. N. Boldyrev, Y. G. Selivanov, V. P. Martovitskii, S. V. Chekalin, and E. A. Ryabov, Physical Review B **97**, 1 (2018).
[47]B. S. Dastrup, J. R. Hall, and J. A. Johnson, Applied Physics Letters **110** (2017), 10.1063/1.4980112.
[48]M. Frenzel, M. Cherasse, J. M. Urban, F. Wang, B. Xiang, L. Nest, L. Huber, L. Perfetti, M. Wolf, T. Kampfrath, X.-Y. Zhu, and S. F. Maehrlein, Science Advances **9**, eadg3856 (2023), https://www.science.org/doi/pdf/10.1126/sciadv.adg3856.
[49]M. Traving, M. Boehme, L. Kipp, M. Skibowski, F. Starrost, E. E. Krasovski, A. Perlov, and W. Schattke, Physical Review B **55**, 392 (1997).
[50]K. K. Kam and B. A. Parkinson, Journal of Physical Chemistry **86**, 463 (1982).
[51]M. Takai, K. Shibata, M. Uemoto, and S. Watanabe, Applied Physics Express **9**, 052206 (2016).
[52]C. Somma, K. Reimann, C. Flytzanis, T. Elsaesser, and M. Woerner, Phys. Rev. Lett. **112**, 146602 (2014).